JOURNAL OF NANOSCOPE
ISSN(P): 2707-711X | ISSN(O): 2788-7456 *Volume 2, Issue 1, June 2021, pp 1-13*

The Effect of Annealing time and Gas flow rate on Optical and Magnetic properties of (Al,Co) co-doped ZnO Nanoparticles by Varying Al Concentration

S. Qaseem[1], M. Naeem[2] *, M. Ikram[3], Rubab Zahira[4]

[1]Department of Physics, Federal Urdu University of Arts, Science and Technology Karachi Pakistan.
[2]Department of Physics, University of Karachi, Pakistan.
[3]Department of Physics, Hazara University, Mansehra 21300, Pakistan.
[4]Department of Physics, Government College University, Faisalabad.
Corresponding Author: naeem.khan@uok.edu.pk

Received: 15 March 2021 **Published:** 30 June 2021

Abstract
The effect of Al, a trivalent substitution was investigated in Co doped ZnO with regards to the role of additional carriers in n-type magnetic semiconductors. Nanoparticle samples of Zn1−xCo0.04AlxO with different Al compositions (x = 0, 0.005, 0.010, 0.015 and 0.020) were annealed at 600 oC for different time (5 hours and 8 hours) and different gas flow rates (25 sccm and 50 sccm). All nanoparticles attained Wurtzite hexagonal structure in a stable form after annealing in forming gas. The effect of annealing time and gas pressure were investigated. Magnetization measurements revealed that air annealed samples displayed paramagnetic properties. Nevertheless, after annealing in forming gas, magnetic moments are stabilized and follow a monotonic trend. Diffuse reflectivity measurements revealed the incorporation of Co2+ ions into the Wurtzite hexagonal lattice. The optical band-gap was found to be increasing with increasing Al concentration of up to 0.01, followed by a decrease with further increase in Al concentration

PACS number (s):
61.05.C-; 65.40. G-; 78.20.-e; 82.20. Kh; 31.10.+z.
Keywords:
Diluted magnetic semiconductors; RTFM; Nanoparticles; Gas flow rate; Forming gas atmosphere.

DOI Number: *10.52700/jn.v2i1.25*

INTRODUCTION

Zinc oxide generally stabilizes in n-type wide bandgap semiconductors with a large exciton binding energy (0.06 eV) [1,2]. This property of zinc oxide is very fascinating as it is useful for optoelectronic devices such as tunable ultraviolet photodetectors, ultraviolet excitonic lasers, field emission displays and transparent conductive windows [3]. Qaseem et al. [4] and Keskenler et al. [5] have reported significant effect of particle size and morphology on the optical band gap, magnetic and resistivity behavior. Incorporation of metals (such as Al, Ag, Cu, Fe and Sn) is considered as an effective way in tuning photoelectrical and magnetic properties of the ZnO nanoparticles [6-9]. Al doping in metal oxide nanoparticles is considered to be one of the potential candidates as a conductive system and transparent metal oxide [10]. Furthermore, many researchers have emphasized that the electrical and optical band gap tuning of similar system can be optimized by electron dopants. Houng et al. [11] reported that Al addition in the ZnRuO system leads to increase conductivity because each Al ion offer free carriers in degenerate semiconductors. Shet et al. [12] achieved an optimum value of photocurrent under visible light by co-doping Al in ZnNO system. Pan et al. [13] investigation of Al co-doped ZnSnO system revealed significance transmittance (91%) with very low resistivity (0.004 Ω.cm). Therefore, it appears that co-doping with Al and Co can be interesting and fruitful because of both Al3+ and Co2+ substitution at Zn2+ site in ZnO system. Such material is called diluted magnetic semiconductor (DMS). For the last two decades, the DMS has taken tremendous attention due to its potential application in spintronics devices. Magnetic, magneto-transport, and optical properties of Al-doped ZnCoO thin films have been studied by M. Venkatesan et al. [14]. Thin films of Co doped ZnO with a range of Al co-doping exhibit a band-edge shift, which varies with carrier concentration ‘n’ as n2/3. Krstulovic et al. explores the possibility of Al doped ZnO nanoparticles as an optoelectronics application [15]. Chaudhary et al. [16] studied the ferromagnetic ordering at room temperature in ZnO:Co nanoparticles. They report the observation and possible explanation of intrinsic room temperature ferromagnetism (RTFM) in chemically synthesized nano-crystalline ZnO:Co samples with cobalt concentration ranging from 1 to 10 at%. They also report the effect of cobalt concentration and processing parameters on the magnetization, structure and phase-purity of nanocrystalline powder

samples. K. P. Bhatti, et al. [17] studied the room temperature ferromagnetism in nano-crystalline ZnO:Co system. In this paper, we present a simple chemical rout to synthesize Al co-doped ZnCoO nanoparticles. Al is incorporated as a trivalent ion in ZnO besides a fixed concentration of Co to tune optical band gap and ferromagnetism. It is reported in literature that Al ions substituted in metal oxides exhibit room temperature ferromagnetism. The observed ferromagnetism is linked with mediated electrons induced by the Al doping. A partially filled 3p levels of try valent Al can produce ion exchange interactions (inter 3p-3p or intra 3s-3p). In the light of above literatures, the existence room temperature magnetic ordering in the proposed DMS in the access of free carriers (electron in this case), it would be highly encouraging to investigate role of electron dopant while already existing magnetic ordering. We choose the base system as cobalt doped ZnO while Al was used to incorporate electron. Furthermore, in order to elucidate the significance of oxygen vacancy defect in stabilizing ferromagnetism, a comparative study of the effect of annealing in reducing atmosphere at two different pressures was carried out. Nanomaterial was chosen instead of bulk materials because of easiness in synthesis. In addition, the real applications of such DMS requires the stabilization magnetic ordering at room temperature in relatively small nanoparticles.

EXPERIMENT

Nanoparticles of Zn0.960Co0.040O, Zn0.955Co0.040Al0.005O, Zn0.950Co0.040Al0.010O, Zn0.945Co0.040Al0.015O and Zn0.940Co0.040Al0.020O were synthesized by heating metal acetates in organic solvent following the previously procedure reported [18]. Hydrated Zinc-acetate, Co-acetate tetrahydrate Co(CH3COO)2.4H2O and Aluminium hydroxide acetate Al(OH)(CH3COO)2 used as initial precursor. All as-prepared nanoparticles were then processed in the presence of forming gas (Ar95%+H5%) atmosphere at 600 oC inside the tabular furnace. Two series of samples named ZCAO-500 and ZCAO-800 were prepared at annealing time 5 hours and 8 hours respectively. The gas flow rate for both sets of samples were fixed at 25 sccm. The crystalline structure was analyzed by using XRD (JDX-11P3A JEOL, Japan). The magnetic measurements were performed on vibrating sample magnetometer (VSM) of Riken Denish Company Ltd, Japan (BHV-50). Optical band gap of these samples was carried out using optical set up of Perkin-Elmer advanced model Lemda-950.

RESULTS AND DISCUSSION

In order to study the effect of aluminum concentration on microstructural properties of Zn1−xCo0.04AlxO nanoparticles of different values of dopant concentration (0, 0.005, 0.010, 0.015, and 0.020) were studied. The XRD patterns of samples ZCAO-500 and ZCAO-800, annealed under forming gas (Ar95%+H5%) at flow rate 25 sccm are shown in Fig.1(a) and Fig.1(d). All the samples were found to be in stabilized hexagonal Wurtzite phase. No extra peaks were observed concerning any secondary pha ses such as CoO and Co metal clusters. The diffraction peaks of nanoparticle are well matched with JCPDS card no. 36–1451. All XRD patterns of ZCAO-500 and ZCAO-800 are almost similar indicating that the structure remains unchanged with increasing annealing time. It can be seen that the diffraction peaks are enhanced and sharpened for ZCAO-800 compared to ZCAO-500, thereby indicating the crystallization and quality of structure were improved at higher annealing time. Scherrer equation is used to estimate crystallite size of the samples [19]. The calculated average particle size of Al undoped sample from most intense peak (101) is 22 nm. However, peak widening is observed with addition of Al in ZnCoO nanoparticles. This peak widening can be attributed to stress in the crystal arising due to substitution of small ionic size of Al3+ (0.53A0) for large ionic size of Zn (0.74 A0). This may however be also due to decrease in size of nanoparticles with Al addition [20]. A careful investigation of XRD patterns indicates a little shifting of the Al doped ZnCoO diffraction peaks towards a higher 2θ value in comparison with those of pure ZnCoO. Furthermore, the lattice parameters (a and c) are found to vary with Al content. The evolution of the lattice parameters (a and c) of ZCAO-500 and ZCAO-800 versus Al concentration are given in Fig.1(b) and Fig.1(e) respectively. It can be seen that the lattice parameters (a and c) of ZCAO-500 and ZCAO-800 nanoparticles decrease with increasing Al content. The systematic decrease in the lattice parameters suggest that the Al ions are well substituted at cation site [20]. Fig. 1(c) and Fig.1(f) represent bright field transmission electron microscopy images of ZCAO-500 and ZCAO-800 nanoparticles. It is clear that most of the particles are spherical with average particle size in the range of 22–40 nm. The corresponding selected area diffraction patterns are given in the inset of Fig.1(c) and Fig.1(f). The symmetric diffraction rings are well matched with the dominant peaks of the XRD pattern. These results further confirm that the nanoparticles are well stabilized in hexagonal Wurtzite structure.

XPS measurements were carried out to determine elemental composition and defect concentration. Fig. 2(a) shows a typical XPS survey scan of ZCAO-500. Fig. 2(b) shows the core line of Zn2p

spectrum. The peak is fitted with two symmetric peaks located at 1021.1 eV, and 1044.3 eV which correspond to Zn2p3/2 and Zn2p1/2 respectively. The characteristic spin orbit splitting peaks of Zn2p suggests that Zn ions exist in +2 oxidized state [21]. Fig.2(c) shows the O1s core spectrum. The asymmetric O1s spectrum is fitted with a linear combination of Lorentzian and Gaussian functions. The peak at lower side (OII: 529.9 eV) corresponds to oxygen ions bonded with host lattice and the peak at higher energy side (OI: 531.4 eV) might be associated with oxygen ions in the oxygen deficient regions within the matrix of ZnO and therefore correlated with the concentration of oxygen vacancies [6]. In addition, a characteristic peak of Al2p (shown in Fig.2(d)) is deconvoluted into two peaks at 74.8.0 eV and 73.6eV. The major part of Al2p peak at 74.8 eV corresponds to Al3+states, which is probably related to Al dopant in hexagonal ZnO lattice. The minor part at 73.6 eV represents neutral Al.

For optical properties, UV-Vis spectroscopy system has been utilized. Optical diffuse reflectance spectra were recorded in the wavelength range of 850 to 250 nm. All spectra were then fitted with the well-known Kubelka-Munk function [22]. Fig. 3(a) shows the reflectance spectra for ZCAO-500 samples with different Al concentrations. Additional peaks labelled as 569 nm, 614 nm, 660 nm are observed for all thef samples. These peaks indicate the electronic transitions due to the crystal-field-splitting of 3d-levels. This splitting is due to the substitution of Co2+ ions in place of Zn2+ ions in hexagonal symmetry [23]. It is clear from the Fig.3(a), that there is a shift in absorption edge to shorter wavelengths (higher energies) and there is an increase in the band gap of Co doped ZnO nanoparticles with the addition of Al. K-M function was used for the measurement of band gap of pure and Al doped samples annealed in forming gas atmosphere for ZCAO-500. Fig. 3 (b) shows the change in bandgap energy with Al content. It is observed that with Al doping band gap of Co doped ZnO increases up to 1.0%Al concentration and after that it starts decreasing. Figure 3(c) shows reflectance spectra taken for ZCAO-800 samples and corresponding energy band gap versus Al content is plotted in Fig. 3(d). It can be seen that the bandgap energy increases first up to 1.0%Al and it starts to decrease up to the 2%Al. Fig. 3(b) and 3(d) show decrease in the optical gap with increase in Al beyond 1.0% Al. The increasing in the band gap up to 1.0%Al might be due to Burstein-Moss effect in which Al ions tend to shift the Fermi level into the conduction band [24]. Nevertheless, the decrease of band gap at higher concentration suggests that excess Al atoms is not activated due to segregation at the grain boundaries. These results are consistent with the results of Kuo, et al. [25]. Similar decrease in

band gap with the increase in Al concentration in Al doped ZnO system is explained by the formation of trapping states below the conduction band with the increase in Al as reported in the published work [26].

To understand the origin of magnetic ordering in our nanoparticles, magnetization versus field (M-H) loops were taken at 300 K with maximum applied field □7 kOe. Room temperature ferromagnetism is observed for samples annealed in forming gas. Figure 4(a) shows M-H curves of the ZCAO-500 annealed in forming gas at 25 sccm. The presence of room temperature in the Co doped ZnO annealed in a forming gas and its absence in the air annealed samples (data not shown here) is now a well- established result. The effect obviously is related to the introduction of additional charge carriers due to the oxygen vacancies and their role in the formation of bound magnetic polarons and possibly in the mediation of the moment between localized Co moments [27]. What is new here is the variation of the moment with the addition of Al in the oxygen reduced samples. As shown in inset of figure 4(a), the moment initially decreases with the addition of aluminum, reaches a minimum, and then again starts to increase. The measurements were repeated for different samples of the same composition and annealed in the same conditions. We note that the variations due to the small amount of the Al introduced into the system produce very significant variations in the moment, almost halving the moment by the addition of 1.0% Al. This shows the extreme sensitivity of the system to chemical and electronic changes brought about by the doping. There may be two reasons for this. Firstly, when Al is added it may get substituted near the cobalt atom. The substitution of Al atom near cobalt atom is possible because hexagonal crystal structure of ZnO is already distorted at the locations where cobalt is already present and thus it favors the formation of new defects in its vicinity. This inhibits the formation of oxygen vacancies and hence reduces the carrier concentration. Secondly, in this low concentration regime Al ions that are n-type dopants are not sufficient to compensate for the loss of carriers due to depleted oxygen vacancies. This trend apparently continues till the minimum of Ms is reached at about 0.5% Al. As moves toward higher concentration of aluminum, the shortage of oxygen vacancies appears to be overcome by the number of additional carriers contributed by the Al and the moment consequently rises. Fig. 4(b) shows the Magnetization versus field plots for samples ZCAO-800. It is observed that moment decreases with initial Al doping unlike the case of ZCAO-500. It steadily begins to rise very soon and reaches almost to a constant value after Al doping of 1.0%, shown in inset of fig. 4(b). In fact, magnetization in Al and Co doped ZnO depends on the ratio of

carrier concentration and transition metal ions. As the cobalt concentration is fixed in our case, this ratio changes with the carrier concentration only. Thus, in low Al concentration regime carriers are low as compared to the pure sample causing a decrease in moment and as Al concentration increases so is the nc/ni ratio and moment increase [20]. It is expected that with increase in the annealing time the number of oxygen vacancies present in the system increases. This in turn increases the number of carriers and hence the value of nc/ni ratio eventually starts increasing at 0.01% concentration of Al compared to ZCAO-800 samples in which this increase starts at 1%Al concentration. As far as the magnetization of the samples is concerned there is no drastic change as compared to the ZCAO-500 samples. This indicates that the total moment is contributed by the Co only and the Al ions act to increase the efficiency of the coupling and moment formation.

Furthermore, the effect of flow rate of forming gas on the magnetization by doubling its pressure (from 25 sccm to 50 sccm) has also been studied. Fig. 5 shows the Magnetization versus field plots for pure ZnCoO and Al doped ZnCoO nanoparticles. With increase in the pressure of the reducing atmosphere, the number of oxygen vacancies is expected to increase in the system. As discussed earlier, the number of oxygen vacancies, are of crucial importance in the case of stabilizing ferromagnetism in Co doped ZnO nanoparticles as evident from the literature. It is significantly observed that while doubling the pressure has a strong positive influence on the moment in the Al un- doped samples it has almost negligible effect on the Al doped samples. The remaining trend is as before viz. the moment rises systematically with Al concentration. Therefore, the observations reconfirm the assertion in the previous sections that at low Al concentrations the effect of Al ions is to primarily prevent the formation of oxygen vacancies, while at higher concentrations the role of the additional carriers due to the Al become dominant. Our observed trend of increase of magnetization with increasing Al concentration, under fixed annealing conditions, is consistent with the results of Xu, et. el. [28].

CONCLUSION

XRD patterns of all the samples showed no extra peaks concerning mixed phases such as CoO or Co metal clusters. It showed no changes in crystal structure in our range of temperature and gas pressure variation during annealing. However peak widening is observed with the addition of Al in Co doped ZnO nanoparticles. This peak widening can be attributed either due to stress in the crystal arising or due to substitution of small size Al ions for large size Zn ions. The variation in

band gap as a function of Al dopant in ZnCoO by reflectance measurements was steadily investigated. The optical band gap increased with the Al concentration until 1.0%, which is associated with the Burstein-Moss effect. The decrease of the optical band gap for $x > 1.0$ has attributed to electron trapping by Al at higher concentrations. It is thus obvious that Al doping even in such a small trace is a powerful means of varying the optical band gap in ZnO. Magnetic measurements of undoped and Al doped samples showed that only the addition of Al i.e., increasing the carrier concentration is not sufficient to stabilize room temperature ferromagnetism, at least in our range of Al doping. The presence of oxygen vacancies is necessary to stabilize ferromagnetism in all samples.

REFERENCES

1. M. M. Jumidali, M. R. Hashim, Super lattices and Microstructures 52 (2012) 33. DOI: 10.1016/j.spmi.2012.04.007
2. H. Chettah, D. Abdi, Thin Solid Films 537 (2013) 119.DOI: 10.1016/j.tsf.2013.04.024
3. Q. Shi, K. Zhou, M. Dai, S. Lin, H. Hou, C. Wei, F. Hu, Vacuum 94 (2013) 81. DOI: 10.1016/j.vacuum.2013.01.008
4. S. Qaseem, S.Rizwan Ali, M. Naeem, Applied Surface Science 331 (2015) 87. DOI: 10.1016/j.apsusc.2015.01.012
5. E. F. Keskenler, G. Turgut, S. Dogan, Superlattices and Microstructures 52 (2012) 107. DOI: 10.1016/j.spmi.2012.04.002
6. S. Qaseem, M. Naeem, S. Rizwan Ali, M. Maqbool & S. Imran Ali, Materials Technology: Advanced Performance Materials 32 (2017) 327. DOI: 10.1080/10667857.2016.1217117
7. J. Sengupta, R. K. Sahoo, C. D. Mukherjee, Materials Letters 83, 84 (2012). DOI: 10.1016/j.matlet.2012.05.130
8. Munir N, Liaqat B, Batool K, Shafiq R, Akhter N, Sattar M, Tariq K. Experimental investigation of low dimensional spin system in metal oxides. JOURNAL OF NANOSCOPE (JN). 2020 Jan 31;1(01).Z. Pan, X. Tian, S. Wu, C. Xiao, Z. Li, J. Deng, G. Hu, Z. Wei, Superlattices and Microstructures 54 (2013) 107. DOI: 10.1016/j.spmi.2012.11.003
10. S. Wilken, V. Wilkens, D. Scheunemann, R. E. Nowak, K. V. Maydell, J. Parisi, H. Borchert, ACS Appl. Mater. Interfaces 7 (2015) 287. DOI: 10.1021/am5061917

11. Nisar M, Umbreen M, Rafique S, Liaqat B, Batool K, Shahzadi I, Zahra Y, Batool H. Optical Properties of ZnS and Effect of Doping with Transition Elements. JOURNAL OF NANOSCOPE (JN). 2020 Jun 22;1(01):21-33.

12. Ayaz Khan S, Azam S, Kanoun MB, Murtaza G, Rani M, Goumri-Said S. Tailoring the electronic structure and optical properties of cadmium-doped zinc oxides nanosheet. Cogent Physics. 2017 Jan 1;4(1):1391734.

13. Z. Pan, X. Tian, S. Wu, X. Yu, Z. Li, J. Deng, C. Xiao, G. Hu, Z. Wei, Applied Surface Science 265 (2013) 870. DOI: 10.1016/j.apsusc.2012.11.139

14. M. U. Venkatesan, P. Stamenov, L. S. Dorneles, R. D. Gunning, B. Bernoux, J. M. Coey, Applied physics letters, 90 (2007) 242508. DOI: 10.1063/1.2748343

15. N. Krstulovic, K. Salamon, O. Budimlija, J. Kova, J. Dasovi, P. Umek, I. Capan, Applied Surface Science 440 (2018) 916. DOI: 10.1016/j.apsusc.2018.01.295

16. S. Chaudhary, K. P. Bhatti, S. Kundu, S. C. Kashyap, D. K. Pandya, MRS Online Proceedings Library Archive, 9572007 (2006). DOI: 10.1557/PROC-0957-K10-01

17. K. P. Bhatti, S. Kundu, S. Chaudhary, S. C. Kashyap and D. K. Pandya Journal of Physics D, Applied Physics, 39 (2006) 4909. DOI: 10.1088/0022-3727/39/23/001

18. M. Naeem, S. K. Hasanain, M. Kobayashi, Y. Ishida, A. Fujimori, S. Buzby, S. I. Shah, Nanotechnology 17 (2006) 2675. DOI: 10.1088/0957-4484/17/10/039

19. B. D. Cullity, Elements of X-ray Diffractions, Addison-Wesley, Reading, MA, 102, (1978)

20. A. Nakrela, N. Benramdane, A. Bouzidi, Z. Kebbab, M. Medles, C. Mathieu, Results in Physics 6 (2016) 133. DOI: 10.1016/j.rinp.2016.01.010

21. F. J. Sheini, Ceram. Int. 38 (2012) 3649. DOI: 10.1016/j.ceramint.2012.01.004

22. G. Kortum, Reflectance Spectroscopy, Springer-Verlag, New York, (1969)

23. M. Naeem and S. K. Hasanain, J. Phys.: Condens. Matter 24 (2012) 245305

24. E. Burstein, Physical Review, 93 (1954) 632. DOI: 10.1088/0953-8984/24/24/245305

25. S. Y. Kuo, W. C. Chen, F. I. Lai, C.P. Cheng, H. C. Kuo, S. C. Wang, W. F. Hsieh, Journal of Crystal Growth 287 (2006) 78. DOI: 10.1016/j.jcrysgro.2005.10.047

26. J. G. Lu, S. Fujita, T. Kawaharamura, H. Nishinaka, Y. Kamada, T. Ohshima, Z. Z. Ye,

Y. J. Zeng, Y. Z. Zhang, L. P. Zhu, H. P. He, Journal of Applied Physics 101 (2007) 083705. DOI: 10.1063/1.2721374

27. S. S. Ismail, A. R. Ainuddin, AIP Conference Proceedings, 2068 (2019) 020101. DOI: 10.1063/1.5089400

28. X. H. Xu, H. J. Blythe, M. Ziese, A. J. Behan, J. R. Neal, A. Mokhtari, R. M. Ibrahim,

A. M. Fox and G. A. Gehring, New Journal of Physics 8 (2006) 135. DOI: 10.1088/1367-2630/8/8/135

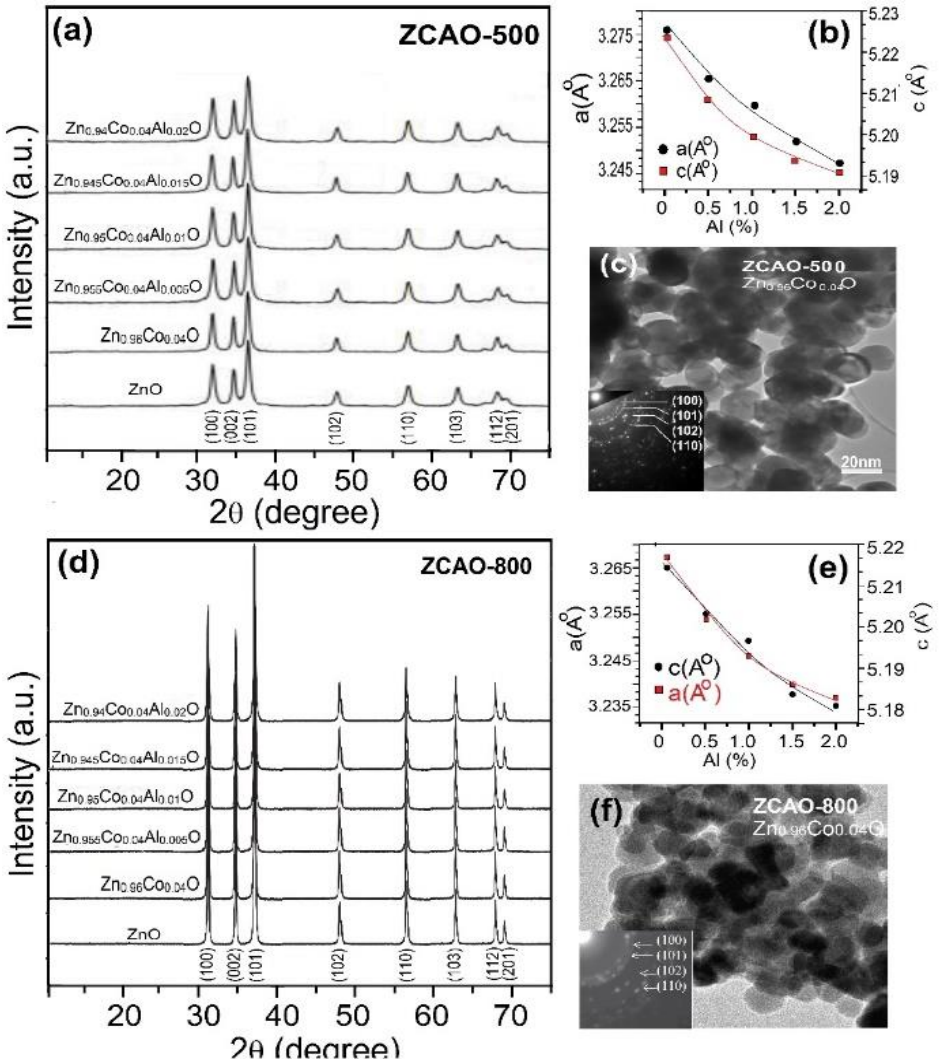

Figure 1: (a) XRD patterns of ZCAO-500; (b) Variation in lattice constant versus Al concentrations; (c) Transmission electron micrograph of Zn0.96Co0.04O nanoparticles; (d) XRD patterns of ZCAO-800; (e) Variation in lattice constant versus Al concentrations; (f) Transmission electron micrograph of Zn0.96Co0.04O nanoparticles

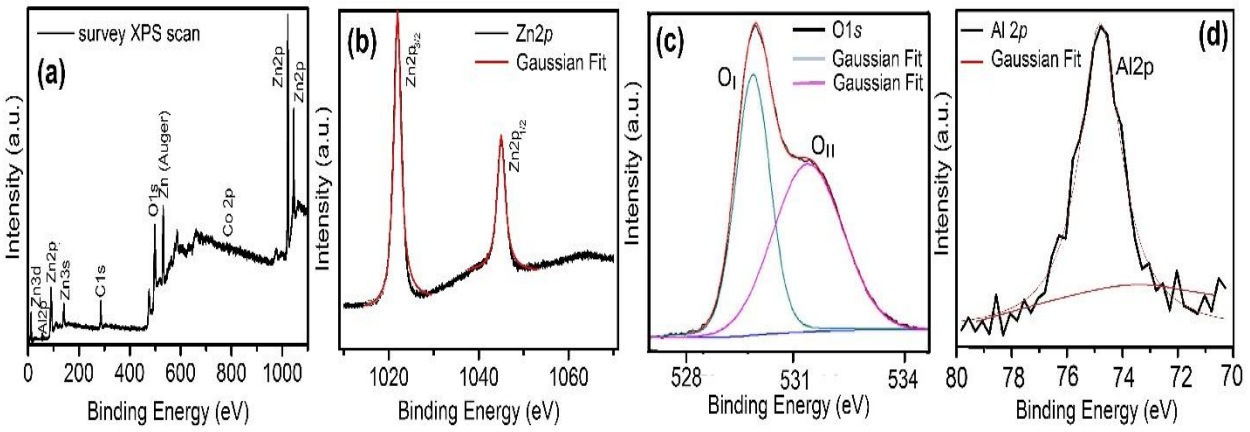

Figure 2: (a) Typical XPS survey scan of ZCAO-500 nanoparticles; High resolution spectra of (b) Zn2p, (c) O1s and (d) Al2p.

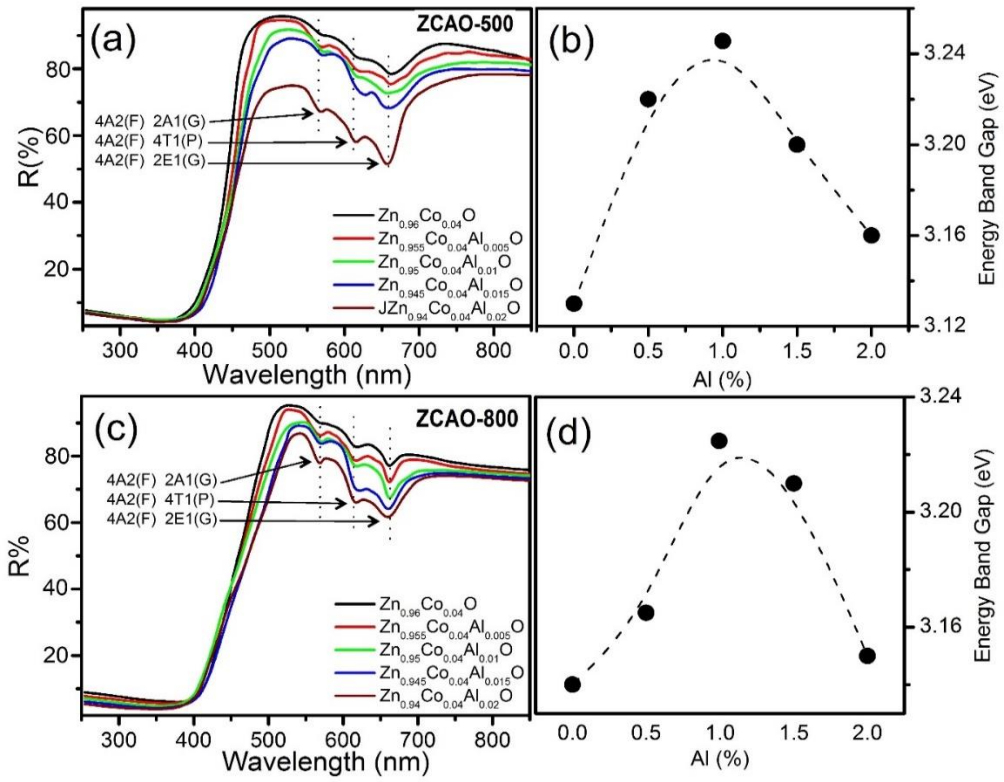

Figure 3: (a) Diffuse reflectance spectra of ZCAO-500; (b) Plot of optical band gap versus Al concentration; (c) Diffuse reflectance spectra of ZCAO-800; (d) Plot of optical band gap versus Al concentration

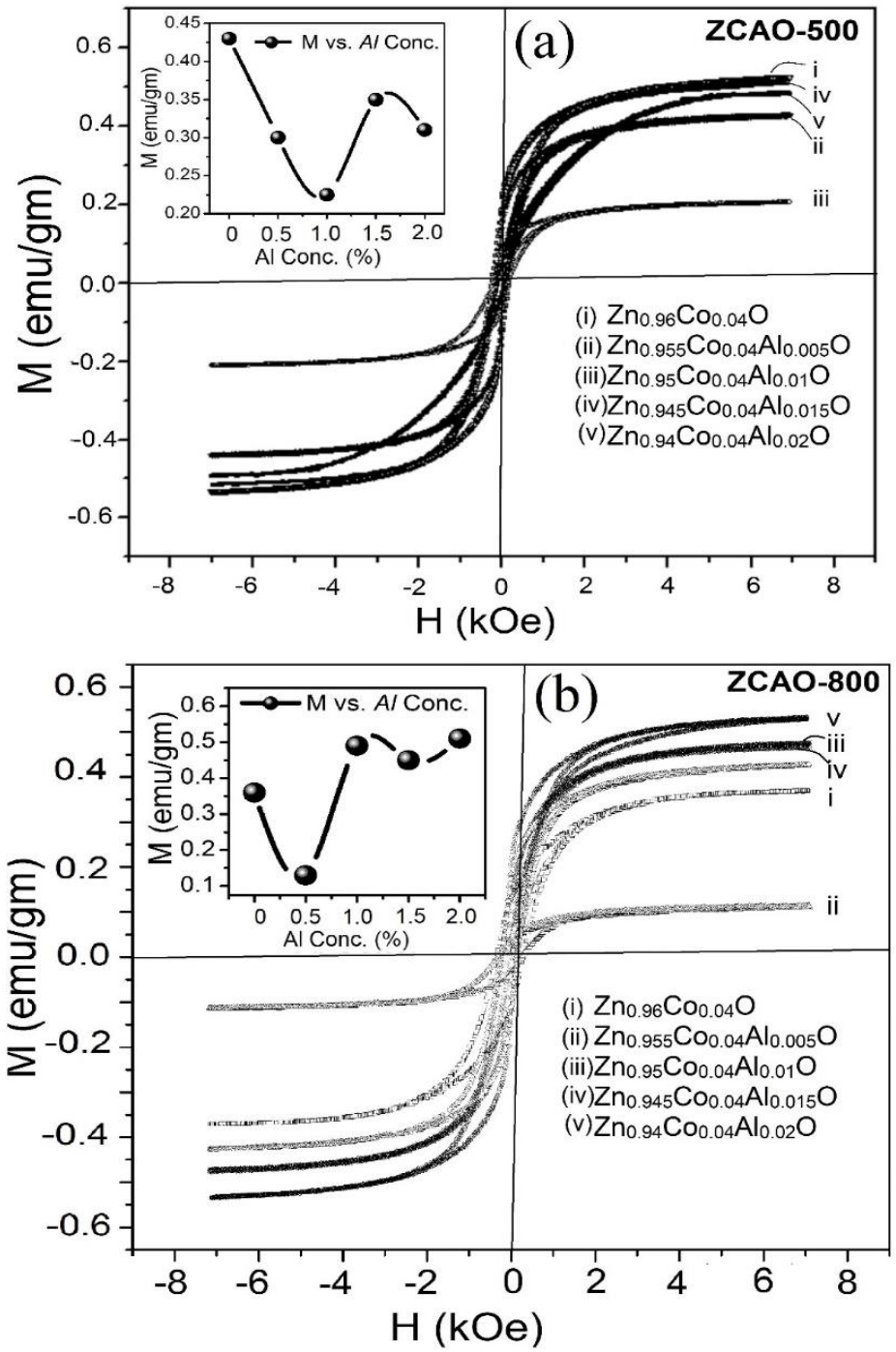

Figure 4: (a) Magnetization versus field behavior of ZCAO-500; Inset of (a) represents magnetization versus Al concentration; (b) Magnetization versus field behavior of ZCAO- 800; Inset of (b) represents magnetization versus Al concentration.

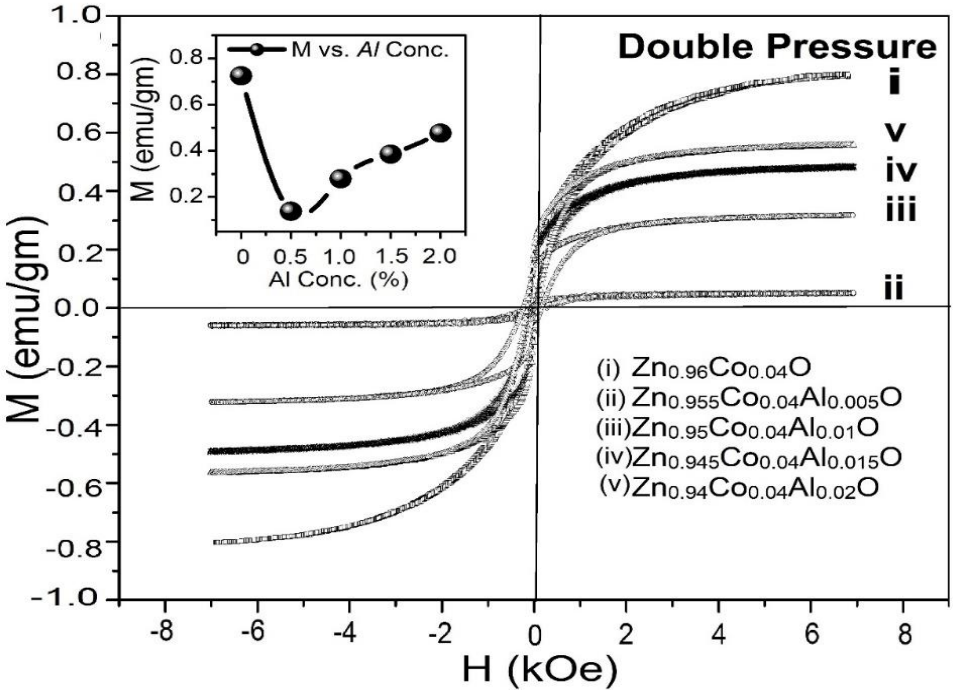

Figure 5: Magnetization versus field behavior of ZCAO-500 at 50sccm; Inset represents magnetization versus Al concentration